FERMILAB-CONF-19-351-DI-LDRD-TD

FERMILAB-CONF-19-351-DI-LDRD-TD

Demonstration of cw accelerating gradients on a cryogen-free, cryocooler conduction-cooled SRF cavity

R C Dhuley[1], M I Geelhoed[1], Y Zhao[2], I Terechkine[1], M Alvarez[1], O Prokofiev[1], and J C T Thangaraj[1]

[1] Fermi National Accelerator Laboratory, Batavia, IL 60502, USA
[2] Euclid Techlabs LLC, Bolingbrook, IL 60440, USA

Abstract. Conduction-cooling of superconducting radiofrequency (SRF) cavities using closed-cycle cryocoolers can lead to compact linear accelerators by eliminating liquid helium and the associated infrastructure. In this paper, we present the first-ever experimental demonstration of continuous wave (cw) accelerating gradients on a niobium SRF cavity that is cooled without using liquid helium. In a newly developed experimental apparatus, a single-cell, 650 MHz niobium cavity was conductively coupled to a 2 W @ 4.2 K pulse tube cryocooler using a high-purity aluminium thermal link. The cw accelerating gradient slightly exceeded 1.5 MV/m, a limit imposed by our RF power supply. Using simple scaling, we project that the niobium cavity when coated with Nb_3Sn and operated on the same experimental setup can produce >10 MV/m cw accelerating gradients.

1. Introduction

Superconducting radiofrequency (SRF) cavities are the workhorse of modern linear particle accelerators built for higher energy physics and basic energy sciences. While there is a continuous push for increasing the accelerating gradients of these cavities (>45 MV/m achieved so far [1]), a number of industrial applications can benefit from SRF accelerators producing low to medium cw gradients. A recent report on energy and environmental applications of accelerators [2] identified the utility of high-power electron beams with electron energy of 0.5-10 MeV in water/sludge decontamination, flue gas clean-up, environmental remediation, and medical waste sterilization. A meter-long or even shorter SRF accelerating structure with average continuous-wave (cw) accelerating gradient up to 10 MV/m can be a potential source of electron beams required for these applications.

The present reliance of SRF accelerators on liquid helium for sustaining superconductivity, however, may cause reluctance to their deployment to the industrial arena. This is because of (a) the decreasing ready-availability and rising cost of helium (b) complex and expensive infrastructure needed to work with liquid helium and (c) hazardous scenarios such as the loss of vacuum, frostbite, and asphyxiation, which are associated with any liquid helium installation. Conduction-cooling using closed-cycle 4 K cryocoolers is an attractive way of operating low-to-medium gradient SRF accelerators, which naturally eliminates liquid helium from them. While there have been a few simulation studies of cryocooler conduction-cooled SRF cavities [3,4], an experimental demonstration does not yet exist. The present work fills this gap by demonstrating cw accelerating gradients >1.5 MV/m on a conduction-cooled niobium SRF cavity and hopes to pave the way for a cryogen-free, compact electron-beam SRF accelerator for energy, environmental, and industrial application as envisioned in

[5]. In this paper, we present the details of our experimental setup and the results of accelerating gradient measurements.

2. Experimental setup

A new experimental setup for accelerating gradient measurement of conduction-cooled SRF cavities has been designed and built at Fermilab. The design of this cryocooler cooled setup is dictated by the following requirements: (1) unlike dc superconducting devices such as a magnet, an SRF cavity dissipates heat during operation (dynamic heating) and therefore needs a high thermal conductance link to connect to the cryocooler 4 K stage. As the dissipation rate increases with cavity temperature, the thermal link must hold the cavity as close to the cryocooler temperature as possible. (2) static heat leak to the cavity near 4 K must be small so that much of the cryocooler 4 K cooling capacity is available to absorb the cavity dynamic dissipation, and (3) the cavity must be housed in a low background magnetic field environment because the dynamic dissipation increases with the amount of trapped magnetic field in the cavity superconductor walls.

2.1. RF cavity, thermal conduction link, and cryocooler

We chose a single-cell, 650 MHz, SRF grade niobium (RRR>300) niobium cavity for the present work. The steps in preparing this cavity for cryocooler conduction-cooled testing are depicted in figure 1.

It is well understood and also shown *via* electromagnetic FEA in figure 1(a) that in the accelerating mode, the magnetic field lines responsible for surface heat dissipation are concentrated near the cavity equator. The cavity surface area per unit axial length is also the largest in this region. As a result, most of the surface dissipation occurs near the cavity equator and a thermal conduction link should be attached near the cavity equator. To provide a flat surface for attaching a thermal link, we electron-beam welded rings of SRF grade niobium on either sides of the cavity equator. A CAD rendering is shown in figure 1(b). A thermal link can be bolted to these welded rings using the holes provided in the azimuthal direction.

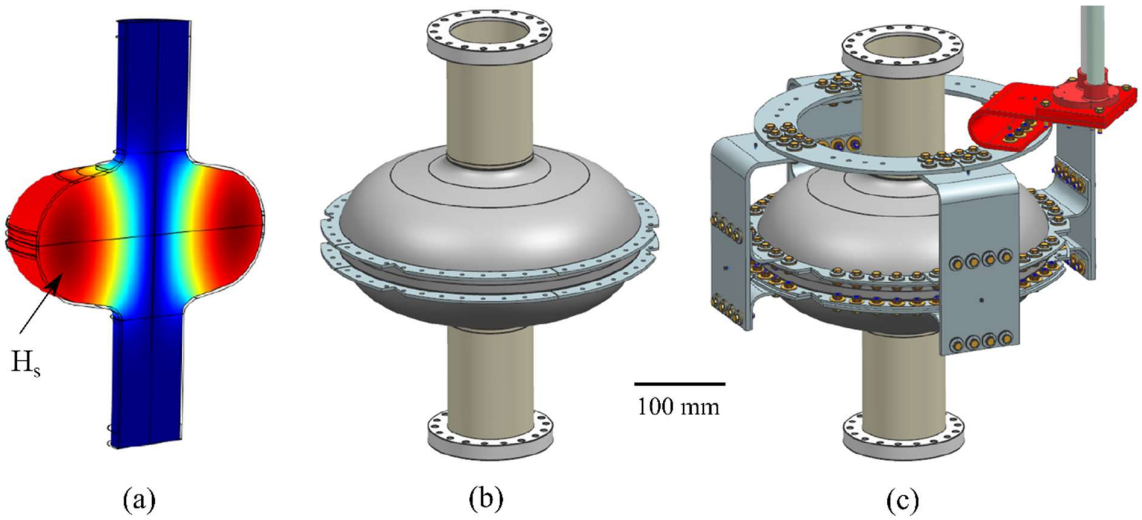

Figure 1. (a) Electromagnetic simulation showing concentration of surface magnetic field around the cavity equator (b) niobium rings welded to the cavity near its equator (b) an aluminium thermal link connecting the cavity to a cryocooler.

Our thermal link is made of high purity 5N aluminium. Pieces were water-jet cut from off-the-shelf aluminium sheets and bended into the thermal link components as displayed in figure 1(c). Going away from the cavity the aluminium link is composed of rings that fasten to the niobium rings on the cavity, elbows, buses with 90-degree bends on one end, a cooling distribution ring, and a bus with a u-bend connected to the cryocooler 4 K stage. Guided by our previous work [6], all the bolted joints within the thermal link were interposed with 5-mil thick indium foil and tightened with a 100 lb-inch torque applied on to 1/4-20 screws with the bolt-tension maintained using Belleville disk springs. The procedure for designing the thermal link and component dimensions can be referred to from our previous report [7]. The cryocooler used in the present work is Cryomech PT420 rated to provide 2 W @ 4.2 K with 55 W @ 45 K.

2.2. The cryostat

Figure 2 shows the components of our cryostat. Referring to the CAD model in figure 2(a), the cryostat is composed of a vacuum vessel, a magnetic shield, a thermal shield, a cavity support structure, and a cavity connected *via* a thermal link to the 4 K stage of a cryocooler.

The vacuum vessel is constructed of stainless steel (SS 304) following the ASME pressure vessel design code and is capable of pumping down to 10^{-8} torr vacuum when the cryocooler is operating at its base temperature. The vessel is 0.8 m in diameter and 1.5 m tall. The magnetic shield is placed inside the vacuum vessel and is designed to offer high permeability at room temperature. To maintain the quality the of background magnetic field, we have taken utmost care of not using magnetic materials inside the magnetic shield. The exceptions are the cryocooler regenerator materials, body of the cryocooler cold-head, and Belleville disc springs used on the thermal contacts. The mu-metal magnetic shield attenuates the background magnetic field at the location of the cavity to below 5 mG in the vertical as well as horizontal directions. The background field can be reduced further using active field compensation coils located outside the vacuum vessel.

Located inside the magnetic shield, the thermal shield comprises of an OFHC copper (top) plate, bolted to a thin walled aluminium 1100 shell with a welded bottom cover. The thermal shield is conductively cooled using flexible copper straps connected to the cryocooler first stage and is wrapped with multilayer insulation to reduce its thermal radiation loading from room temperature. All of the cavity instrumentation cables (wiring for thermometers, heaters, fluxgates, as well as RF cables) are heat sunk to the thermal shield top plate. The thermal shield hangs from the vacuum vessel top plate on non-magnetic Ti64 alloy threaded rods. The cavity and the conduction link hangs on separate Ti64 threaded rods also attached to the vacuum vessel top plate. The cavity support rods are heat sunk to the thermal shield top plate to reduce conduction heat leak through them from room temperature to 4 K. With the thermal shield operating near 50 K, we estimate the cavity support heat leak to be less than 150 mW to 4 K.

Figure 2(b) shows the cavity as connected to the cryocooler 4 K stage using the aluminium link. The assembly hangs below the thermal shield top plate. The black RF cables coming in through the thermal shield top plate, seen as unattached in the picture, are meant to connect to RF ports on the ends of the beam-pipes of the cavity.

2.3. RF power and control system

The RF power and control system provides up to 10 W of cw power at 650 MHz and is capable of measuring the forward, reflected, and transmitted powers from the cavity. The system also samples the cavity resonance at 1 MHz and rapidly adjusts the source frequency to lock on to the cavity resonance. Figure 3 shows a block diagram of the RF power and control system.

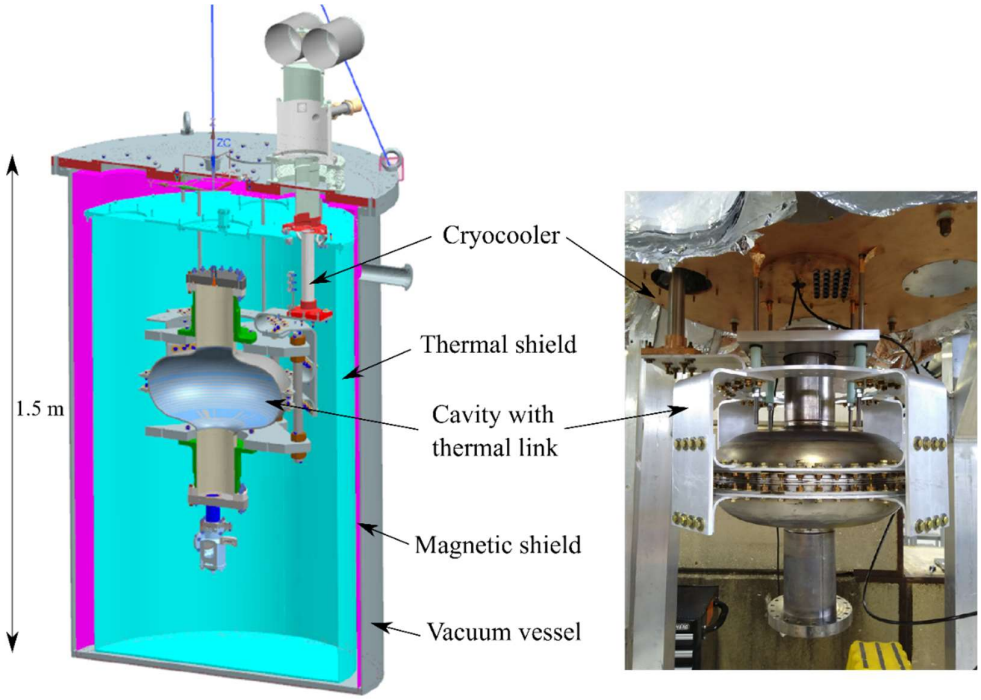

(a) (b)

Figure 2. Experimental setup (a) a CAD rendering showing the cryostat components and (b) photograph of the cavity and thermal link shown hanging below the thermal shield top plate.

The following quantities are required to determine the quality factor and accelerating gradient of an SRF cavity: power incident at the cavity input (forward power), power reflecting at the cavity input (reflected power), power at the cavity output (transmitted), and decay time constant of the cavity once the forward power is shut off. The forward and reflected powers are measured off calibrated diodes, whose voltage output is recorded by an oscilloscope within the RF system. The transmitted power is calibrated using the feedback intermediate frequency (IF) signal voltage. The cavity decay time constant is obtained by shutting off the forward power, recording the decay portion of the transmitted power, and then fitting a time-exponential function to the decaying transmitted power data. All the above measurements and fitting are executed in a LabView routine.

Cavity-source resonance locking is achieved in the following way: the FPGA module controls the RF frequency to stabilize the RF phase at a setpoint based on its feedback value. The IQ signal and local oscillator signal are synchronized by sharing 10 MHz reference clock and are mixed by signal up-converter which generates RF signal, after amplification, up to 10 W RF signal can be delivered to the input of cavity. Then attenuated feedback RF signal whose frequency is down-converted by a mixer generates a feedback IQ (IF) signal, which gives amplitude and phase information of RF signal. Depending on a fast feedback PI control loop in the FPGA, the RF output frequency can be adapted instantly to make feedback phase stabilize at phase setpoint.

3. Results and discussion

3.1. Cooldown characteristics

The cryostat attained steady base temperature within 24 hours of starting the cryocooler. At steady state, the cryocooler stage-1 reached 28 K, the thermal shield top plate attained 32 K, while the

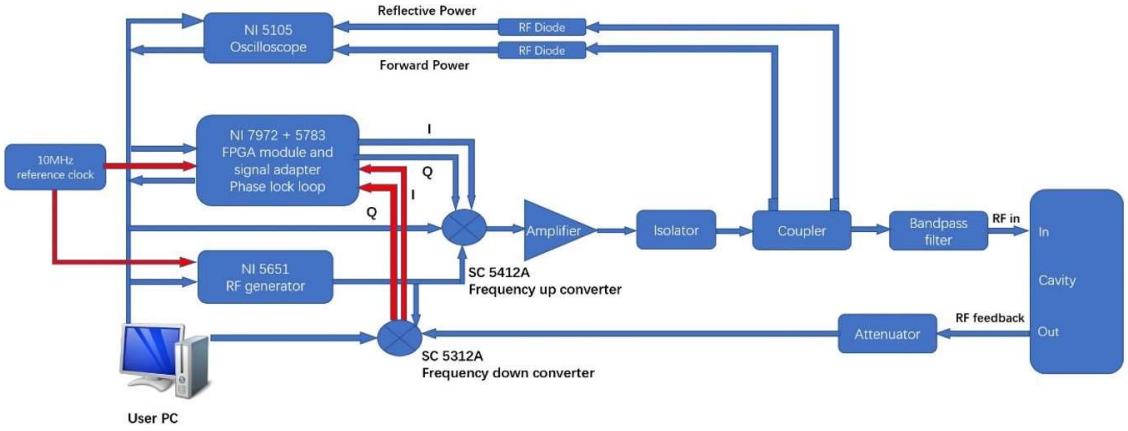

Figure 3. Block diagram of the RF power and control system used for the present work.

cryocooler stage 2 cooled to 2.95 K. A separate cooling capacity measurement of the cryocooler indicated that 2.95 K on stage-2 corresponds to ≈450 mW of heat leak. We estimate about 150 mW of this leaks through the cavity support structure and the remaining ≈300 mW through the RF cables attached on the ends of the cavity beam-pipes. Thermometers mounted on the cavity at three locations on its elliptically curved surface read between 5 and 5.8 K. The spread presumably is because of improper thermal contact between the thermometers and the curved surface of the cavity. We do believe that the cavity is operating considerably warmer than the cryocooler because of the static heat leak that has to flow through the cavity body, the thermal link, and into the cryocooler. Identification of the sources and mitigating static heats leaks is currently in progress.

3.2. Quality factor and accelerating gradient measurement on the niobium cavity

Figure 4 shows a plot of cavity quality factor, Q_0 *vs.* accelerating gradient, E_{acc} obtained *via* steady state measurement of forward, reflected, and transmitted powers and decay measurement of transmitted power. We have followed the measurement and calculation procedure as outlined in [8] to determine Q_0 and E_{acc} as well as their uncertainties. The forward power was increased in steps, which each time yielded higher E_{acc} but a lower Q_0. The fall in Q_0 can be explained based on the fact that the rising E_{acc} causes greater dissipation in the cavity, which means an increased heat load on the cryocooler. The cryocooler thereby warms up and also causes the cavity to warm up. The rise in the cavity temperature results in higher surface resistance, R_s and a corresponding drop in Q_0 (as $Q_0 \propto 1/R_s$). Such behaviour is unique to a cryocooler-cooled SRF cavity and may not be seen with a cavity operated in 2 K superfluid helium. In the latter, the high diffusivity and heat capacity of the superfluid helium bath provides an isothermal condition to the cavity, not causing significant change in the Q_0 at gradients observed in the present study.

The data represented with filled circles in figure 4 had no applied heat load on the cryocooler stage-1 while the unfilled circles represent the data obtained after supplying 55 W to the stage-1 of the cryocooler. Higher E_{acc} are obtained by loading the cryocooler stage-1, a process known to enhance the stage 2 cooling capacity. This enhancement allows tolerating higher dissipation in the cavity, which is equivalent to higher E_{acc} according to the relation $E_{acc} = \sqrt{P_{diss} / [R_s(T) * (r/Q) * G]}$, where P_{diss} is dissipated power; r/Q and G are constants purely dependent on cavity geometry. The highest E_{acc} of ~1.6 MV/m measured during the experiments is not limited by cavity quench but by the RF power supply limit and input coupling at the cavity. At this limit the forward power is 10 W, reflected power is ≈6.0 W, transmitted power is ≈2 mW, which yields ≈3.5 W of dissipated power. A larger

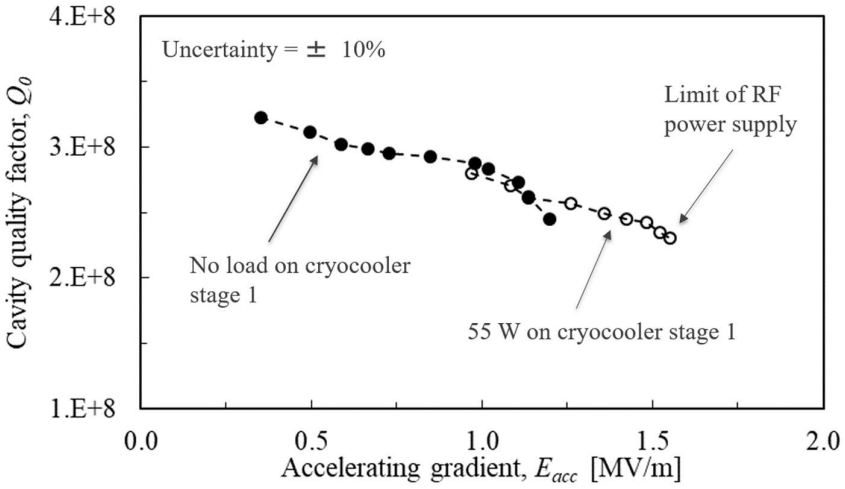

Figure 4. Cavity quality factor, Q_0 *vs.* accelerating gradient, E_{acc} measured on a single cell, 650 MHz niobium cavity, conductively cooled using a Cryomech PT 420 cryocooler.

fraction of forward power can be fed into the cavity by improving the input coupling, which is planned for the next stage of our experiments.

3.3. Projections for a 650 MHz Nb_3Sn coated niobium cavity

A thin layer of Nb_3Sn coating on a niobium cavity's RF surface produces orders of magnitude lower surface resistance than a bare niobium cavity around 4 K temperature [9]. Consequently, a coated cavity will yield a much higher accelerating gradient for a given level of dissipated power (or available cooling power). Therefore, a conduction-cooled Nb_3Sn cavity should show accelerating gradients much higher than 1.6 MV/m on our experimental setup. The experiments with a Nb_3Sn coated cavity are underway but below are our performance predictions.

To predict the achievable accelerating gradient, it is first necessary to estimate the average temperature of the cavity RF surface to be able to determine its surface resistance. We calculated the surface resistance of our niobium cavity using the relation $R_s(T) = G / Q_0(T)$, where G=265 Ω and $Q_0(T)$ is that plotted in figure 4. For this $R_s(T)$, the RF surface average temperature is then back-calculated using the numerical code SRIMP [10]. The calculated average temperature of the RF surface, $T_{cavity,RF}$ is plotted against E_{acc} in figure 5. For a comparison, we also plot the measured cryocooler stage-2 temperature, $T_{cryocooler}$. We note that at the highest E_{acc}, $T_{cryocooler}$ ≈5.1 K and $T_{cavity,RF}$ ≈5.7 K.

Our projections for the Nb_3Sn coated cavity use $T_{cryocooler}$ ≈5.1 K, which means that the coated cavity is dissipating the same power as the uncoated cavity (dissipated power equals the heat flow into the cryocooler, which is a unique function of its cold-head temperature). We further take $T_{cavity,RF}$ ≈5.7 K for the coated cavity, which can essentially be realised using our existing thermal link subjected to the heat flow corresponding to $T_{cryocooler}$ ≈5.1 K. Using SRIMP, we calculate the temperature dependent BCS surface resistance for Nb_3Sn around 5.7 K to find that it is nearly three orders of magnitude smaller than that of niobium. Figure 6 shows this calculation. Another component of the surface resistance is its temperature independent residual resistance that depends on the Nb_3Sn coating quality and factors such as trapped magnetic flux in the RF layer [9]. The lowest demonstrated value of the residual resistance is ≈10 nΩ. The total surface resistance including this residual is also plotted in

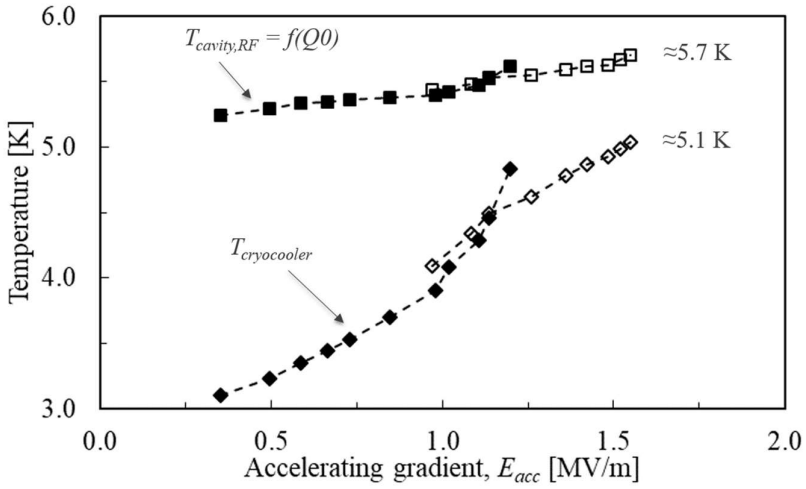

Figure 5. Cryocooler stage 2 temperature and cavity RF surface average temperature as a function of the accelerating gradient.

figure 6 for comparison and we notice this to be still very small than that of niobium. We consider two arbitrary cases in which the Nb_3Sn residual resistance is five and ten-fold worse than 10 nΩ, which may result from a bad quality coating and/or large amount of trapped magnetic flux. The resulting surface resistance is still an order of magnitude lower than that of niobium.

Using the relation $E_{acc} \propto 1/\sqrt{R_s(T)}$ for a given dissipation level and the highest gradient of 1.5 MV/m measured on our niobium cavity, we present in Table 1 the accelerating gradients projected for a Nb_3Sn coated cavity. With the existing experimental setup, a gradient as high as 11.5 MV/m is foreseen for a coated cavity with 10 nΩ residual surface resistance. A ten-fold worse residual resistance in Nb_3Sn would still produce 5 MV/m.

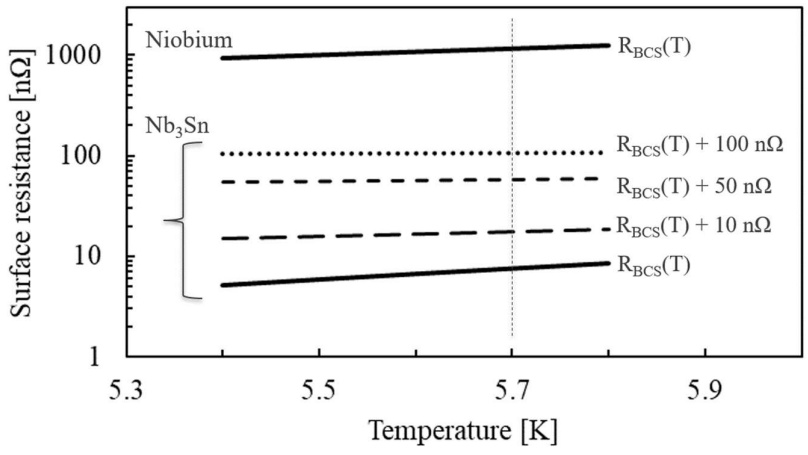

Figure 6. Comparison of surface resistance of niobium and Nb_3Sn around 5.7 K. The temperature dependent $R_{BCS}(T)$ is calculated using the SRIMP code [10].

Table 1. Projected E_{acc} for a Nb_3Sn coated, single cell, 650 MHz cavity using our existing thermal link and the PT420 cryocooler.

RF surface resistance at 650 MHz in Nb_3Sn [nΩ]	E_{acc} [MV/m]
≈20 (residual = 10)	11.5
≈60 (residual = 50)	6.5
≈110 (residual = 100)	5.0

4. Summary and outlook

Using a newly developed cryogen-free setup cooled by a 2 W @ 4.2 K cryocooler, we have demonstrated a cw accelerating gradient in excess of 1.5 MV/m on a single-cell, 650 MHz niobium SRF cavity. This gradient can be pushed further by improving the thermal management in our setup, for example by reducing the 4 K static heat leak. Nonetheless, our analysis and projections show that a Nb_3Sn coated cavity with the existing setup can produce >10 MV/m gradients. The present results provide the first-ever experimental evidence of cryogen-free SRF cavity operation, which we hope will take the SRF accelerator technology a step closer to its deployment in industrial electron beam accelerators.

5. References

[1] Grassellino A *et al* 2017 *Supercond. Sci. Technol.* **30** 094004.
[2] Report of 2015 *Workshop on Energy and Environmental Applications of Accelerators,* ed S Henderson and T Waite.
[3] Ciovati G *et al* 2018 *Phys. Rev. Accel. Beams* 21 091601.
[4] Holzbauer J P and Nassiri A 2014 *Nuclear Instruments and Methods in Physics Research A* **767** 407.
[5] Kephart R *et al* 2015 *Proc. SRF2015 (Whistler, BC, Canada)* p 1468.
[6] Dhuley R C, Geelhoed M I and Thangaraj J C T 2018 *Cryogenics* **93** 86.
[7] Dhuley R C, Kostin R, Prokofiev O, Geelhoed M I, Nicol T H, Posen S, Thangaraj J C T, Kroc T K, and Kephart R D 2019 *IEEE Transactions on Applied Superconductivity* **29(5)** 0500205.
[8] Melnychuk O, Grassellino A, and Romanenko A 2014 *Review of Scientific Instruments* **85** 124705.
[9] Posen S, Liepe M, and Hall D L 2015 *Applied Physics Letters* **106** 082601.
[10] SRIMP code available online at https://www.classe.cornell.edu/~liepe/webpage/researchsrimp.html

Acknowledgments

This manuscript has been authored by Fermi Research Alliance, LLC under Contract No. DE-AC02-07CH11359 with the U.S. Department of Energy, Office of Science, Office of High Energy Physics. The authors thank Fermilab's SRF group members for their insights and assistance during various stages of this work.